

Fast Particle Destabilization of TAE Modes

C. Z. Cheng, N. N. Gorelenkov* and C. T. Hsu

Princeton Plasma Physics Laboratory,
P. O. Box 451, Princeton, New Jersey 08543 USA

Abstract

High- n TAE modes are studied based on a kinetic model that includes full thermal ion finite Larmor radius effects, trapped electron collisions and fast particle instability drive. Lower KTAE modes are shown to be non-existent. Like TAE modes, upper KTAE modes are shown to exist due to thermal ion FLR effects in the dissipationless limit. Dissipation effects on the stability of both TAE and upper KTAE modes can be treated perturbatively. However, due to their extended mode structure in the ballooning space, upper KTAE modes usually remain stable or weakly unstable even with large fast particle free energy. On the other hand, TAE modes can be strongly destabilized. A new resonant TAE mode (RTAE) can be excited when the fast particle drive is significantly large. The RTAE mode is a beam-like mode with its frequency determined mainly by the wave-particle resonance condition. The frequency of the RTAE mode can be much less than the TAE gap frequency and may be interpreted as the BAE observed in DIII-D experiments. As plasma β increases, the TAE, RTAE and kinetic ballooning modes strongly couple; the TAE mode changes into the RTAE mode and eventually connects to the kinetic ballooning mode. Numerical results and analytical analysis on the stability of the RTAE and KTAE modes will be presented and compared with the TAE mode stability.

*Permanent address: Troitsk Institute for Innovative and Fusion Research, Troitsk, Moscow region, Russia, 142092

1. INTRODUCTION

Since the theoretical prediction of the toroidal (or toroidicity-induced) Alfvén eigenmode (TAE) in toroidal devices [1, 2], much progress has been achieved in understanding the stability of TAE modes in the presence of energetic ions. Plasma resistivity leads to the existence of an additional TAE type mode, the periodic shear Alfvén waves [1]. Inclusion of thermal ion finite Larmor radius (FLR) effects modifies the wave spectrum of periodic shear Alfvén waves to form the KTAE modes [3]. In addition, thermal ion FLR effects also enhance the collisional damping of the TAE and KTAE modes, which are called the radiation damping [4, 5]. Recently, we have also identified a new resonant TAE mode (RTAE), which is a beam-like mode with its frequency determined mainly by the wave-particle resonance condition and is excited when the fast particle drive is significantly large. The frequency of the RTAE mode can be less than the TAE gap frequency and may be identified as the BAE modes observed in DIII-D experiments [6, 7]. As the plasma β increases, the TAE, RTAE and kinetic ballooning modes strongly couple; the TAE mode changes into the RTAE mode and eventually connects to the kinetic ballooning mode. Previous studies [3–5, 8] have mostly concentrated on perturbative analyses of TAE stability and have ignored the coupling among TAE, KTAE, RTAE and kinetic ballooning modes. It is thus essential to study the stability properties of TAE, KTAE and RTAE modes and their coupling to kinetic ballooning modes by employing non-perturbative analyses and by including FLR effects and accurate dissipation mechanisms.

Theoretical studies and experimental observations have indicated that medium- to high- n TAE modes, where n is the toroidal mode number, will be most unstable in fusion devices such as ITER, JT-60U, JT-60SU, DIII-D, JET, and TFTR [7, 9, 10]. Physics requirements for a successful stability analysis should include:

1. Thermal ion finite Larmor radius (FLR) effects for radiative damping and continuum damping.
2. Landau resonances of thermal plasma ions, electrons and fast ions.
3. Collisional damping of thermal electrons.

4. Energetic/ α particle pressure gradient drive with velocity distribution including finite drift orbit effects for fusion products and pitch angle scattering for beam ions.
5. Non-perturbative analysis of driving and damping mechanisms when they are large enough to affect TAE, KTAE, RTAE and kinetic ballooning mode structure or spectrum.
6. Realistic numerical equilibria to provide reasonable Alfvén continuum and gap structure.
7. Realistic plasma profiles to provide accurate stability calculation.

These requirements need to be implemented in two-dimensional high- n stability codes as well as global stability codes such as *NOVA-K* [11] to be used for studying experimental results and designing fast particle experiments. Our strategy has been to improve the global *NOVA-K* code and to develop a new two-dimensional high- n code and to establish overlapping domain of validity in the medium- n range ($n \simeq 10 - 40$) between these two codes.

In the paper we will study the stability of high- n TAE, KTAE and RTAE modes and their coupling to kinetic ballooning modes in the lowest order in the high- n WKB-ballooning formalism. We present an eigenmode formulation based on gyro-kinetic equations. We will study the effects of thermal ion FLR, fast particle pressure gradient drive, thermal ion pressure gradient and trapped electron collisional damping on TAE, KTAE and RTAE mode spectra and growth rates. The eigenmode structure and growth rate will be found non-perturbatively by solving the high- n eigenmode equation in the WKB-ballooning space. The validity condition of the perturbative method is discussed. This work is the first step toward developing a comprehensive and efficient two-dimensional high- n TAE stability code based on the WKB-ballooning formalism.

The paper is organized as follows. In Sec. 2 we present the gyrokinetic formulation and obtain eigenmode equations for studying TAE, KTAE, RTAE and kinetic ballooning modes. In Sec. 3 we discuss the result of numerical analysis of the eigenmode equations. In Sec. 4 we summarize the main results.

2. HIGH-N EIGENMODE EQUATIONS

2.1. Gyrokinetic-Maxwell Equations

We shall consider a WKB representation of perturbed quantities which are proportional to $e^{i(S-\omega t)}$, where S is the WKB eikonal of the perturbed quantities and ω is the wave frequency. Including full FLR effects the perturbed particle distribution function can be expressed in terms of the rationalized MKS unit as

$$\begin{aligned} \delta f &= \frac{q}{M} \frac{\partial F}{\partial \mathcal{E}} \Phi + \frac{q}{MB} \frac{\partial F}{\partial \mu} \left[\Phi + \frac{i}{\omega} \mathbf{v}_{\parallel} \cdot \nabla (\Phi - \Psi) \right] (1 - J_0 e^{iL}) \\ &- \frac{q}{MB} \frac{\partial F}{\partial \mu} \frac{v_{\perp} \delta B_{\parallel}}{|\nabla S|} J_1 e^{iL} - \frac{q}{M} \frac{\partial F}{\partial \mathcal{E}} \left(1 - \frac{\omega_{*}^T}{\omega} \right) \Phi J_0 e^{iL} + g e^{iL}, \end{aligned} \quad (1)$$

where F is the particle equilibrium distribution function, M is the particle mass, q is the particle charge, B is the magnetic field intensity, $\mathcal{E} = v^2/2$, $\mu = v_{\perp}^2/2B$, the subscripts \parallel and \perp represent parallel and perpendicular components to the equilibrium magnetic field, $L = (|\nabla S| v_{\perp} / \omega_c) \sin \varphi$, φ is the particle gyro-phase angle between ∇S and \mathbf{v}_{\perp} , S satisfies $\mathbf{B} \cdot \nabla S = 0$ and will be determined later, J_l is the l -th order Bessel function of the argument $|\nabla S| v_{\perp} / \omega_c$, $\omega_c = qB/M$ is the cyclotron frequency, Φ is the electrostatic potential, Ψ is the parallel electric field potential with $\mathbf{E}_{\parallel} = -\nabla_{\parallel} \Psi$, δB_{\parallel} is the parallel perturbed magnetic field, and g is the nonadiabatic part of the perturbed distribution function. Note that the vector potential, defined by $\mathbf{A} = \mathbf{A}_{\parallel} - iA_{\perp} \mathbf{B} \times \nabla S / (B|\nabla S|)$, is related to Φ , Ψ and δB_{\parallel} by $\omega \mathbf{A}_{\parallel} = -i\nabla_{\parallel} (\Phi - \Psi)$ and $\delta B_{\parallel} = |\nabla S| A_{\perp}$. Based on the WKB-ballooning formalism the lowest order gyrokinetic equation [12,13] for g in the low frequency ($\omega \ll \omega_c$) limit is given by

$$\begin{aligned} (\omega - \omega_d + i\mathbf{v}_{\parallel} \cdot \nabla_{\parallel})g &= -\frac{q}{M} \frac{\partial F}{\partial \mathcal{E}} \left(1 - \frac{\omega_{*}^T}{\omega} \right) \\ &\times \left[(\omega_d \Phi - i\mathbf{v}_{\parallel} \cdot \nabla_{\parallel} \Psi) J_0 + \frac{\omega v_{\perp}}{|\nabla S|} J_1 \delta B_{\parallel} \right], \end{aligned} \quad (2)$$

where $\omega_{*}^T = \mathbf{B} \times \nabla S \cdot \nabla F / (B\omega_c \partial F / \partial \mathcal{E})$, $\omega_d = -(\mathbf{B} \times \nabla S / B\omega_c) \cdot (v_{\parallel}^2 \boldsymbol{\kappa} + \mu \nabla B)$ is the magnetic drift frequency, and $\boldsymbol{\kappa}$ is the magnetic field curvature. Note

that the dissipative effects such as wave-particle resonance and particle collision are included in g .

Using Eq. (1) the quasineutrality condition provides the condition to determine the parallel electric field and is given by

$$\begin{aligned} & \sum_j \int d^3v \frac{q_j^2}{M_j} \left[\frac{\partial F_j}{\partial \mathcal{E}} \left(1 - \frac{\omega_{*j}^T}{\omega} \right) + \frac{1}{B} \frac{\partial F_j}{\partial \mu} \right] (1 - J_0^2) \Phi \\ & + \sum_j \int d^3v \frac{q_j^2}{M_j} \frac{\partial F_j}{\partial \mu} \frac{v_\perp \delta B_\parallel}{|\nabla S|} \left(\frac{|\nabla S| v_\perp}{2\omega_{cj}} - J_0 J_1 \right) + \sum_j \int d^3v q_j g_j J_0 = 0, \end{aligned} \quad (3)$$

where the summation over j is over all particle species.

The perpendicular component of the Ampère's law determines the parallel perturbed magnetic field and is given by

$$\begin{aligned} \mathbf{B} \cdot \delta \mathbf{B}_\parallel + \sum_j \int d^3v \frac{q_j B v_\perp}{|\nabla S|} J_1 \left[\left(g_j - \frac{q_j}{M_j} \frac{\partial F_j}{\partial \mathcal{E}} \left(1 - \frac{\omega_{*j}^T}{\omega} \right) \Phi J_0 \right) \right. \\ \left. - \frac{q_j}{M_j B} \frac{\partial F_j}{\partial \mu} \left(J_0 \Phi + \frac{v_\perp \delta B_\parallel}{|\nabla S|} J_1 \right) \right] = 0. \end{aligned} \quad (4)$$

By multiplying Eq. (2) with particle charge, integrating it over the velocity space and summing it over all species, the parallel component of the Ampère's law (vorticity equation) reduces to

$$\begin{aligned} & \mathbf{B} \cdot \nabla \left[\frac{\sigma |\nabla S|^2}{B^2} \mathbf{B} \cdot \nabla (\Phi - \Psi) \right] \\ & + \omega \sum_j \int d^3v \left[\frac{q_j^2}{M_j} \frac{\partial F_j}{\partial \mathcal{E}} \frac{\omega_{*j}^T v_\perp^2 \delta B_\parallel}{2\omega_{cj}} - q_j \omega_{dj} J_0 \left(g_j - \frac{q_j}{M_j} \frac{\partial F_j}{\partial \mathcal{E}} \left(1 - \frac{\omega_{*j}^T}{\omega} \right) \Phi J_0 \right) \right] \\ & + \omega^2 \sum_j \int d^3v \frac{q_j^2}{M_j} \left[\frac{\partial F_j}{\partial \mathcal{E}} \left(1 - \frac{\omega_{*j}^T}{\omega} \right) + \frac{1}{B} \frac{\partial F_j}{\partial \mu} \right] \\ & \times \left[(1 - J_0^2) \Phi + \frac{v_\perp \delta B_\parallel}{|\nabla S|} \left(\frac{|\nabla S| v_\perp}{2\omega_{cj}} - J_0 J_1 \right) \right] = 0, \end{aligned} \quad (5)$$

where

$$\sigma = 1 + \sum_j \int d^3v \frac{q_j^2}{M_j B} \frac{\partial F_j}{\partial \mu} \frac{v_\parallel^2 (1 - J_0^2)}{|\nabla S|^2}.$$

In the small FLR limit $\sigma \simeq 1 + (P_{\perp} - P_{\parallel})/B^2$, where P_{\parallel} and P_{\perp} are the parallel and perpendicular equilibrium pressures, respectively.

Equations (3)-(5) constitute the basic gyrokinetic eigenmode equations for studying high- n TAE, KTAE, RTAE and kinetic ballooning modes. To complete the formulation of the eigenmode equations one needs to determine the nonadiabatic perturbed particle distribution. In general, exact solutions of Eq. (2) can not be obtained analytically and must be computed numerically for each magnetic field geometry. However, in this paper we are interested in studying the properties of TAE, KTAE and RTAE modes and their coupling to kinetic ballooning modes. Therefore, we shall consider simplified solutions of the gyrokinetic equation for our purpose. In addition, simplifying assumptions on the FLR effects in the adiabatic terms will also be made to obtain MHD fluid-like terms.

To proceed we shall consider that the fast particle density is much smaller than the thermal plasma density, but the fast particle pressure is on the same order as the thermal plasma pressure. Then we can neglect fast particle perturbed density terms because of small fast particle density. The plasma β is assumed to be small so that the parallel perturbed magnetic field terms can be neglected in the quasineutrality equation. For thermal ions we assume that $|v_{\parallel}\nabla_{\parallel}|, \omega_{di} \ll \omega$, and from Eq. (2) we have

$$g_i \simeq 0, \quad (6)$$

where we have neglected the thermal ion resonance contribution which may provide additional Landau damping. Note that full FLR effects in the perturbed thermal ion distribution will be retained in the thermal ion density response and are important in determining the existence of KTAE modes and the corresponding collisional radiation damping effects.

For electrons we shall neglect FLR effects and assume that $|v_{\parallel}\nabla_{\parallel}| \gg \omega, \omega_{de}, \nu_e$, where ν_e is the electron collision frequency. Then, from Eq. (2) we see that to the lowest order in $(\omega/|v_{\parallel}\nabla_{\parallel}|)$ g_e is proportional to Ψ , which will lead to the collisional-radiative damping [14]. If we define

$$g_e = \hat{g}_e + \frac{q_e}{M_e} \frac{\partial F_e}{\partial \mathcal{E}} \left(\frac{1 - \omega_{*e}^T}{\omega} \right) \Psi, \quad (7)$$

then \hat{g}_e represents the next order correction in $(\omega/|v_{\parallel}\nabla_{\parallel}|)$ and contains the electron dissipation effects. The equation for \hat{g}_e and its solution will be given

in Sec. 2.2. Integrating over the velocity space for thermal ions and electrons with Maxwellian distributions the parallel electric field potential Ψ can be obtained from the quasineutrality equation, Eq. (3), and is given by

$$\Psi \simeq \frac{q_i T_e (1 - \omega_{*pi}/\omega)}{q_e T_i (1 - \omega_{*e}/\omega)} (1 - \Gamma(b_i)) \Phi + \frac{T_e}{q_e} \frac{\delta \hat{n}_e}{n_e}, \quad (8)$$

where $\delta \hat{n}_e = \int d^3v \hat{g}_e$, $\rho_i = \sqrt{2T_i/M_i/\omega_{ci}}$, $\Gamma(b_i) = I_0(b_i) \exp(-b_i)$, $b_i = |\nabla S|^2 \rho_i^2/2$, I_0 is the modified Bessel function of the zeroth order, the particle diamagnetic drift frequencies are given by $\omega_{*pj} = -(\rho_j^2 \omega_{cj}/B) \mathbf{B} \times \nabla S \cdot \nabla \ln P_j$, $\omega_{*j} = -(\rho_j^2 \omega_{cj}/B) \mathbf{B} \times \nabla S \cdot \nabla \ln n_j$, and P_j and n_j are the equilibrium pressure and density of species j , respectively.

By ignoring FLR effects in the pressure terms the perpendicular component of the Ampere's law, Eq. (4), is simplified to

$$\mathbf{B} \cdot \delta \mathbf{B} + \sum_j \delta p_{\perp j} = 0, \quad (9)$$

where the perturbed pressures are given by

$$\begin{pmatrix} \delta p_{\parallel j} \\ \delta p_{\perp j} \end{pmatrix} \simeq \left[-\frac{i \mathbf{B} \times \nabla \Phi}{\omega B^2} \cdot \tilde{\nabla} + \frac{\mathbf{B} \cdot \delta \mathbf{B}}{B} \left(\frac{\partial}{\partial B} \right)_{\psi} \right] \begin{pmatrix} P_{\parallel j} \\ P_{\perp j} \end{pmatrix} + \begin{pmatrix} \delta \hat{p}_{\parallel j} \\ \delta \hat{p}_{\perp j} \end{pmatrix}, \quad (10)$$

$\tilde{\nabla} = \nabla - (\partial/\partial B)_{\psi}$, the subscript ψ denotes that the operator is acting along the magnetic surface, and the nonadiabatic perturbed pressures are given by

$$\begin{pmatrix} \delta \hat{p}_{\parallel j} \\ \delta \hat{p}_{\perp j} \end{pmatrix} = M_j \int d^3v g_j \begin{pmatrix} 2(\mathcal{E} - \mu B) \\ \mu B \end{pmatrix}. \quad (11)$$

Ignoring FLR effects and making use of Eq. (9) and the equilibrium relation

$$\nabla_{\perp}(P_{\perp} + B^2/2) = \sigma B^2 \boldsymbol{\kappa}, \quad (12)$$

the second term in Eq. (5) can be reduced to

$$\begin{aligned} \omega \sum_j \int d^3v \left[\frac{q_j^2}{M_j} \frac{\partial F_j}{\partial \mathcal{E}} \frac{\omega_{*j}^T v_{\perp}^2 \delta B_{\parallel}}{2\omega_{cj}} - q_j \omega_{dj} J_0 \left(g_j - \frac{q_j}{M_j} \frac{\partial F_j}{\partial \mathcal{E}} \left(1 - \frac{\omega_{*j}^T}{\omega} \right) \Phi J_0 \right) \right] \\ \simeq \frac{\omega \mathbf{B} \times \boldsymbol{\kappa} \cdot \nabla S}{B^2} (\mathbf{B} \cdot \delta \mathbf{B} - \sum_j \delta p_{\parallel j}). \end{aligned} \quad (13)$$

Then, the vorticity equation, Eq. (5), reduces to

$$\begin{aligned} \mathbf{B} \cdot \nabla \left[\frac{\sigma |\nabla S|^2}{B^2} \mathbf{B} \cdot \nabla (\Phi - \Psi) \right] + \frac{n_i M_i \omega^2}{B^2} \frac{[1 - \omega_{*i}/\omega]}{\rho_i^2/2} [1 - \Gamma_0(b_i)] \Phi \\ + \left(\frac{\mathbf{B} \times \boldsymbol{\kappa} \cdot \nabla S}{B^2} \right) \left(\frac{\mathbf{B} \times \tilde{\nabla} P_{\parallel}}{B^2} + \frac{\sigma \mathbf{B} \times \tilde{\nabla} P_{\perp}}{\tau B^2} \right) \cdot \nabla S \Phi \\ - \left(\frac{\omega \mathbf{B} \times \boldsymbol{\kappa} \cdot \nabla S}{B^2} \right) \sum_j (\delta \hat{p}_{\parallel j} + \sigma \delta \hat{p}_{\perp j} / \tau) = 0, \end{aligned} \quad (14)$$

where $\sigma = 1 + (P_{\perp} - P_{\parallel})/B^2$ and $\tau = 1 + B^{-1}(\partial P_{\perp}/\partial B)_{\psi}$. Note that in obtaining Eq. (14) we have neglected the fast particle contribution in the third term of Eq. (5) and have made use of Eqs. (9) and (10).

Equations (8) and (14) form a coupled set of eigenmode equations for solving Φ and Ψ along the field lines and the eigenvalue ω . We also need to obtain the nonadiabatic contributions of perturbed electron density, $\delta \hat{n}_e$, and perturbed particle pressures, $\delta \hat{p}_{\parallel}$ and $\delta \hat{p}_{\perp}$. The eigenmode equations include effects of pressure anisotropy, parallel electric field, full thermal ion FLR, trapped electron collision, and wave resonances with fast particles.

2.2. Trapped Electron Contribution

Keeping the electron collision and the parallel electric field, considering small FLR limit, assuming $\omega \gg \omega_{de}$, and using Eq. (7), the gyrokinetic equation, Eq. (2), for electron reduces to

$$(\omega + iv_{\parallel} \nabla_{\parallel} - iC) \hat{g}_e \simeq -\frac{q_e}{M_e} \frac{\partial F_e}{\partial \mathcal{E}} \left(1 - \frac{\omega_{*e}^T}{\omega} \right) (\omega \Psi + \omega_k \Phi), \quad (15)$$

where C is the Lorentz collisional operator, $\omega_k = (\mathbf{B} \times \boldsymbol{\kappa} \cdot \nabla S / B \omega_{ce}) (\sigma v_{\perp}^2 / 2\tau + v_{\parallel}^2)$ and for trapped electrons it can be approximated as $\omega_k \simeq \omega_{kT} (M_e \mathcal{E} / T_e)$, $\omega_{kT} = (\mathbf{B} \times \boldsymbol{\kappa} \cdot \nabla S / B) (T_e / M_e \omega_{ce})$. Following Rosenbluth et al. [15] and Mikhailovskii [16] we solve Eq. (15) using the orderings $|v_{\parallel} \nabla_{\parallel}| \gg \omega \gg C$. Without collisions \hat{g}_e is given to the lowest order in (ω/ω_b) , where ω_b is the bounce frequency, by

$$\hat{g}_{e0} = \frac{q_e F_e}{T_e} \left(1 - \frac{\omega_{*e}^T}{\omega} \right) \overline{\left(\Psi + \frac{\omega_k}{\omega} \Phi \right)}, \quad (16)$$

where the bar means a drift orbit averaging. Note that only trapped electrons contribute to Eq. (16). Including collisions we can write $\hat{g}_e = \hat{g}_{e0}(1 + y)$ and the equation for y is given by the bounce-averaged collisional equation [15]

$$\left[\omega - i \left(\frac{T_e}{M_e \mathcal{E}} \right)^{3/2} \frac{2\bar{\nu}}{L(\lambda)} \frac{\partial}{\partial \lambda} D(\lambda) \frac{\partial}{\partial \lambda} \right] y \simeq 0, \quad (17)$$

where $\lambda = \mu B_0 / \mathcal{E}$, B_0 is the equilibrium magnetic field at the magnetic axis of the plasma column, $L(\lambda) = \oint d\theta / \sqrt{1 - \lambda/h}$, $h = B_0/B$, $D(\lambda) = \oint d\theta \lambda \sqrt{1 - \lambda/h}$, $\bar{\nu} = \nu [Z_{eff} + G(\sqrt{M_e \mathcal{E}/T_e})]$, $G(z) = (e^{-z^2}/z\sqrt{\pi}) + (2/\sqrt{\pi})(1 - 1/2z^2) \int_0^z e^{-t^2} dt$, Z_{eff} is the effective ion charge, $\nu = \omega_{pe}^2 q_e^2 \sqrt{M_e} (2T_e)^{-3/2} \ln \Lambda$, ω_{pe} is the electron plasma frequency, and Λ is the Coulomb logarithm. We shall consider a circular tokamak in the large aspect ratio limit with $B \simeq B_0/(1 + \epsilon \cos \theta)$, where ϵ is the inverse aspect ratio. Introducing the new variable $\xi = (\lambda - 1 + \epsilon)/2\epsilon$ we have

$$L(\lambda) = \frac{8}{\sqrt{2\epsilon}} K(\sqrt{1 - \xi}); \quad D(\lambda) = 8\sqrt{2\epsilon} [E(\sqrt{1 - \xi}) - \xi K(\sqrt{1 - \xi})], \quad (18)$$

where K and E are elliptic integrals of the first and second kind, respectively.

Near the barely trapped singular layer $\xi \simeq 0$, $K \simeq 0.5 \ln(16/\xi)$, $E \simeq 1$ and Eq. (17) is reduced to

$$\left[\frac{d^2}{d\xi^2} - i \frac{\epsilon \omega}{2\bar{\nu}} \left(\frac{M_e \mathcal{E}}{T_e} \right)^{3/2} \ln \left(\frac{16}{\xi} \right) \right] y \simeq 0, \quad (19)$$

which can be solved with the boundary conditions that $y = -1$ for barely trapped electrons with $\xi = 0$ and $y = 0$ for deeply trapped electrons with $\xi \simeq 1$. Because $\epsilon \omega / \bar{\nu} \gg 1$, a WKB solution of Eq. (19) can be obtained and is given by

$$y \simeq -\exp \left(-\int_0^\xi \hat{\sigma}(\xi') d\xi' \right), \quad (20)$$

where $\hat{\sigma} = (1 - i) \left[\epsilon \omega / 4\bar{\nu} (M_e \mathcal{E}/T_e)^{3/2} \ln(16/\xi) \right]^{1/2} \gg 1$. Effectively \hat{g}_e can also be written in the convenient form

$$\hat{g}_e \simeq \hat{g}_{e0} \left[1 - \frac{(1+i)}{2} \left(\frac{T_e}{M_e \mathcal{E}} \right)^{3/4} \left(\frac{\bar{\nu}}{\nu} \right)^{1/2} \xi_0 \delta(\xi - \xi_0) \right], \quad (21)$$

where ξ_0 gives the characteristic pitch angle width of the trapped electron domain that effectively interacts with the waves and is obtained to be small with $\xi_0 \simeq [(4\nu/\epsilon\omega)/\ln(8\sqrt{\epsilon\omega/\nu})]^{1/2} \ll 1$.

The contribution of trapped electrons to the nonadiabatic perturbed electron density in the quasineutrality equation, Eq. (8), is obtained from Eqs. (7) and (21) and is given by

$$\delta\hat{n}_e \simeq \frac{q_e n_e}{T_e} \left\{ \left\langle \overline{\Psi} + \frac{\overline{\omega_{kT}}}{\omega} \overline{\Phi} \right\rangle - i\sqrt{2\epsilon} \left(C_1 \overline{\Psi} + C_2 \frac{\overline{\omega_{kT}}}{\omega} \overline{\Phi} \right) \left[\left(\cos^2 \frac{\theta}{2} - \xi_0 \right) \frac{4\epsilon\omega}{\nu} \ln \left(8\sqrt{\frac{\epsilon\omega}{\nu}} \right) \right]^{-1/2} \right\}, \quad (22)$$

where $\sqrt{2\epsilon}$ represents the trapped electron fraction, and for $Z_{eff} = 1$ the constants $C_1 = 1.61$ and $C_2 = 2.35$ result from integrations over the Maxwellian distribution, and the angular brackets mean the velocity space integration over the trapped electron Maxwellian distribution.

The nonadiabatic perturbed electron perpendicular pressure in the vorticity equation, Eq. (14), is given by

$$\delta\hat{p}_{\perp e} \simeq \frac{q_e P_e}{T_e} \left\{ \left\langle \frac{M_e \mathcal{E}}{T_e} \left(\overline{\Psi} + \frac{\overline{\omega_{kT}}}{\omega} \overline{\Phi} \right) \right\rangle - i\sqrt{2\epsilon} \left(C_2 \overline{\Psi} + C_3 \frac{\overline{\omega_{kT}}}{\omega} \overline{\Phi} \right) \left[\left(\cos^2 \frac{\theta}{2} - \xi_0 \right) \frac{4\epsilon\omega}{\nu} \ln \left(8\sqrt{\frac{\epsilon\omega}{\nu}} \right) \right]^{-1/2} \right\}, \quad (23)$$

where $C_3 = 6.46$.

With the nonadiabatic trapped electron contributions, Eqs.(22) and (23), the eigenmode equations, Eqs.(8) and (14), are integro-differential equations. To further simplify the nonadiabatic trapped electron density and pressure responses to TAE-like modes we will restrict our analysis for eigenmodes with even parity and determine the interaction between the wave and trapped electrons through terms $\overline{\Phi}, \overline{\Psi}$ in Eqs.(22) and (23). We make use of analytical solutions of the eigenmode equation [1] that TAE-like modes have poloidal structure $\Phi \sim A(\theta) \cos(\theta/2)$, where $A(\theta)$ is a slowly varying functions. Then, averaging over the trapped electrons leads to $\langle \overline{\Psi} \rangle = \langle (M_e \mathcal{E}/T_e) \overline{\Psi} \rangle \simeq \sqrt{2\epsilon} \Psi$, $\langle (\overline{\omega_{kT}}/\omega) \overline{\Phi} \rangle \simeq \sqrt{2\epsilon} \omega_{kT0} \Phi/\omega$, $\langle (\overline{M_e \mathcal{E} \omega_{kT}}/\omega T_e) \overline{\Phi} \rangle_{tr} \simeq 5\sqrt{2\epsilon} \omega_{kT0} \Phi/2\omega$, and $\omega_{kT0} \simeq -T_e |\nabla_{\theta} S|/M_e \omega_{ce} R$. For barely trapped electrons we perform the drift

orbit averaging and obtain $\overline{\Psi}/\sqrt{\cos^2 \theta/2 - \xi_0} \simeq (2\pi/\ln 8\sqrt{\epsilon\omega/\nu}) \Psi \equiv \lambda_1 \Psi$ and $\overline{\Phi \cos \theta}/\sqrt{\cos^2 \theta/2 - \xi_0} \simeq 4\pi\sqrt{\nu/\epsilon\omega} (\ln 8\sqrt{\epsilon\omega/\nu})^{-3/2} \Phi \equiv \lambda_2 \Phi$. Then, the nonadiabatic trapped electron density and pressure responses from trapped electrons can be written in the form

$$\begin{aligned} \delta \hat{n}_e &\simeq \sqrt{2\epsilon} \frac{q_e n_e}{T_e} \left[\Psi + \frac{\omega_k T_0}{\omega} \Phi - i \frac{C_1 \lambda_1 \Psi + C_2 \lambda_2 \Phi \omega_k T_0 / \omega}{((4\epsilon\omega/\nu) \ln 8\sqrt{\epsilon\omega/\nu})^{1/2}} \right], \\ \delta \hat{p}_{\perp e} &\simeq \sqrt{2\epsilon} \frac{q_e P_e}{T_e} \left[\Psi + \frac{5\omega_k T_0}{2\omega} \Phi - i \frac{C_2 \lambda_1 \Psi + C_3 \lambda_2 \Phi \omega_k T_0 / \omega}{[(4\epsilon\omega/\nu) \ln 8\sqrt{\epsilon\omega/\nu}]^{1/2}} \right]. \end{aligned} \quad (24)$$

These formula represent the average responses in poloidal angle from trapped electrons.

2.3. Fast Particle Contribution

To obtain an analytical solution of the gyrokinetic equation for fast particles we assume that $\omega, \omega_d \gg |v_{\parallel} \nabla_{\parallel}|$, which allows a local solution of the treatment of the gyrokinetic equation. This assumption is appropriate for trapped particles produced in the perpendicular neutral beam injection (NBI) in tokamaks. Then, from Eq. (2) the perturbed fast particle distribution function is approximately given as

$$g_h \simeq -\frac{q_h}{M_h} \frac{\partial F_h}{\partial \mathcal{E}} \left(1 - \frac{\omega_{*h}^T}{\omega} \right) \frac{\omega_{dh} J_0 \Phi}{\omega - \omega_{dh}}. \quad (25)$$

We will assume that the fast particle equilibrium distribution function is given by a slowing-down distribution

$$F_h = \frac{c_h(r)}{\mathcal{E}^{3/2} + \mathcal{E}_*^{3/2}} \delta(\lambda - \lambda_0) H(\mathcal{E} - \mathcal{E}_{h0}), \quad (26)$$

where $c_h(r)$ is a normalization constant, H is the Heaviside step function, λ_0 is the fast particle birth pitch angle, \mathcal{E}_{h0} is the fast particle birth energy and \mathcal{E}_* is the slowing down characteristic energy when the effect of electrons on

thermalization of fast particles is comparable with the effect of thermal ions. Typically, $\mathcal{E}_{h0} \gg \mathcal{E}_*$ for alpha particles. Then, the perturbed fast particle pressure contribution is given by

$$\delta\hat{p}_{\parallel h} + \delta\hat{p}_{\perp h} \simeq P_h \frac{\omega_{*h}}{\omega} \left\{ 1 + \frac{\omega}{\omega_{*h}} \left(\frac{\omega_{*h}}{\omega_{dh}} - \frac{1}{3} \right) \left[\ln \left(\frac{\omega_{dh}}{\omega} - 1 \right) + i\pi\Sigma \right] \right\} \frac{q_h \Phi}{\mathcal{E}_{h0}}, \quad (27)$$

where the quantities ω_{*h} and ω_{dh} must be taken at the fast particle birth energy \mathcal{E}_{h0} and the birth pitch angle λ_0 , $\Sigma = 0$ for $\omega_r < 0$ and $\omega_r > \omega_{dh}$, and for $0 \leq \omega_r \leq \omega_{dh}$ we have $\Sigma = (0, 1, 2)$ corresponding to $Im(\omega)(>, =, <)$, respectively. Note that in obtaining Eq. (27) we have neglected fast particle FLR and finite banana orbit width effects and assumed that $\mathcal{E} \gg \mathcal{E}_*$.

2.4. High- n Eigenmode Equation

For tokamak equilibria the magnetic field can be expressed as $\mathbf{B} = \nabla\psi \times \nabla(\zeta - q(\psi)\theta)$, where $2\pi\psi$ is the poloidal flux between the magnetic axis and a constant $\psi < \text{surface}$, $q(\psi)$ is the safety factor, and θ and ζ are generalized poloidal and toroidal angles with a period of 2π , respectively. To the lowest order in $(1/n)$ in the WKB-ballooning formalism the local high- n eigenmode equations are to be obtained by choosing $S = n[q(\psi)\theta - \zeta - \int dq\theta_k(\psi)]$, where θ_k is to be determined from a higher order radially non-local analysis [17, 18]. Assuming the analytical $s - \alpha_p$ equilibrium model for circular cross section tokamaks [17–19], we have $b_i = b_{\theta i}[1 + h(\theta)^2]$, $\mathbf{B} \times \boldsymbol{\kappa} \cdot \nabla S = -(B_0 |\nabla_\theta S| / R) [\cos \theta + h(\theta) \sin \theta]$, where $h(\theta) = s(\theta - \theta_k) - \alpha_p \sin \theta$, $b_{\theta i} = k_\theta^2 \rho_i^2 / 2$, $k_\theta = |\nabla_\theta S| \simeq nq/r$, $s = rq'/q$ is the magnetic shear, $\alpha_p = -2P'Rq^2/B_0^2$, P is the total plasma pressure, r is the minor radius. In general we have to study the lowest order high- n eigenmode equation for all θ_k values to perform a two-dimensional eigenmode analysis. However, we shall choose $\theta_k = 0$ in the paper because the most unstable modes are usually related to $\theta_k = 0$.

In the eigenmode equations, Eqs. (8) and (14), we have included thermal ion FLR effects for collisional-radiative damping due to trapped electron collision and energetic ion pressure gradient drive. Substituting the trapped electron density response, Eq.(24), into the quasineutrality condition, Eq. (8), we obtain the parallel electric field potential

$$\Psi \simeq \frac{\Phi}{1 - \sqrt{2\epsilon_0} + i\delta_1} \left[\frac{q_i T_e}{q_e T_i} (1 - \Gamma(b_i)) \right], \quad (28)$$

where $\delta_1 = C_1 \lambda_1 \left((\nu/2\omega)/\ln 8\sqrt{\epsilon\omega/\nu} \right)^{1/2}$, $\sqrt{2\epsilon_0}$ represents the fraction of effective trapped electrons, and we have neglected thermal electron and ion diamagnetic drift effects.

The vorticity equation for high- n modes, Eq. (14), reduces to

$$\begin{aligned} \frac{\partial}{\partial\theta} [1 + (s\theta - \alpha_{pc} \sin\theta)^2] \frac{\partial(\Phi - \Psi)}{\partial\theta} + \frac{\omega(\omega - \omega_{*i})}{\omega_A^2} \frac{(1 + 2\hat{\epsilon} \cos\theta)[1 - \Gamma_0(b_i)]}{b_{\theta i}} \Phi \\ + [\cos\theta + (s\theta - \alpha_p \sin\theta) \sin\theta] \\ \times \left\{ \alpha_{pc} \Phi - \alpha_{ph} \frac{\omega}{\omega_{*h}} \left(\frac{\omega_{*h}}{\omega_{dh}} - \frac{1}{3} \right) \left[\ln \left(\frac{\omega_{dh}}{\omega} - 1 \right) + i\pi\Sigma \right] \Phi \right. \\ \left. - \frac{\omega q \sqrt{\beta_i}}{\omega_A k_{\theta} \rho_i} (1 - \sqrt{2\epsilon_0} + i\delta_2) \Psi \right\} = 0, \end{aligned} \quad (29)$$

where $\hat{\epsilon} \simeq 2(r/R + \Delta'(r))$, $\Delta(r)$ is the Shafranov shift, $\alpha_{pc} = -2P'_c R q^2 / B_0^2$ is for the core thermal plasma contribution, $\alpha_{ph} = -2P'_h R q^2 / B_0^2$ is for the fast ion contribution, R is the major radius, $\omega_A = V_A / qR$, $V_A^2 = B_0^2 / n_i M_i$, $\beta_{i,e}$ are the thermal ion and electron beta, $\omega_{*i} / \omega_A = q k_{\theta} \rho_i \beta_i^{1/2} / 2\epsilon_n$, $\epsilon_n = L_{pi} / R$, L_{pi} is the thermal ion pressure gradient scale length, $\omega_{dh} / \omega_A = q k_{\theta} \rho_i \beta_i^{1/2} (T_h / T_i) G(\theta)$, $T_h = M_h \mathcal{E}_{h0}$, $G(\theta) = 1$ for bounce-averaged magnetic drift frequency and $G(\theta) = \cos\theta + h(\theta) \sin\theta$ for local magnetic drift frequency, $\omega_{*h} = (T_h \epsilon_n / T_i \epsilon_h) \omega_{*i}$, $\epsilon_h = L_{ph} / R$, L_{ph} is the fast ion pressure gradient scale length, and $\delta_2 = C_2 \lambda_1 \left((\nu/2\omega)/\ln 8\sqrt{\epsilon\omega/\nu} \right)^{1/2}$. For typical tokamak parameters we expect $\delta_2 > \delta_1 \geq 0.1$ for TAE modes. The last term in Eq. (29) that is proportional to β_e is due to trapped electron perturbed pressure. Note that the results presented in the next section is insensitive to the choice of $G(\theta)$.

3. RESULTS

The eigenmode equation, Eq. (29), with the parallel electric field potential given by Eq. (28) has been solved non-perturbatively for high- n TAE-like modes using the shooting method in the infinite ballooning θ variable space. The results have cleared up several important concepts about the stability properties of the TAE, KTAE, RTAE and kinetic ballooning modes. In particular, we have shown the non-existence of lower KTAE modes, the perturbative nature of the collision-radiative damping of the TAE and KTAE

modes, the existence of a resonant type TAE mode (RTAE) due to fast particle resonance, and the coupling between TAE, RTAE and kinetic ballooning modes.

3.1. Existence of TAE and KTAE

It is well known, that in toroidal plasmas two neighboring poloidal harmonics interact due to finite toroidicity and form the TAE modes [1, 2]. Plasma resistivity leads to the existence of an additional TAE type mode, the periodic shear Alfvén wave (PSAW) [1]. PSAWs have two branches with eigenfrequencies given by $\omega \simeq (\omega_A/2)\{1 \pm \hat{e} + (2N+1)c\eta^{1/2}\exp[i(3\pi/2 \pm \pi/4)]\}$, where $N = 0, 1, \dots$ corresponds to different eigenstates, c is a positive real number, and η is the inverse of the magnetic Reynold's number. In the limit $\eta \rightarrow 0$ the lower branch accumulates at the lower continuum gap boundary and the upper branch accumulates at the upper continuum gap boundary. Inclusion of full thermal ion finite Larmor radius (FLR) effects in the resistive MHD model modifies the wave spectrum of PSAWs to form the KTAE modes [3]. Because $b_{\theta i} \gg \eta$ for typical tokamak parameters, the FLR effects takes over and the upper PSAWs move into upper KTAEs with almost purely real frequencies and the lower PSAWs move into lower KTAEs with almost purely imaginary frequencies. However, the resistive MHD model is not accurate for nearly collisionless plasmas such as in the tokamak core region and we consider a more accurate kinetic treatment of electron collision in this paper. We find that the lower KTAEs do not exist as a result of employing a more accurate model of parallel electric field that involves FLR effects.

We first study the solutions of TAE and upper KTAE and the nonexistence of lower KTAE by employing the high- n eigenmode equations, Eqs. (28) and (29) by ignoring pressure contributions from trapped electron and thermal and fast ions, i.e., by setting $\alpha_{pc} = \alpha_{ph} = \beta_e = 0$. We also ignore the trapped electron dissipation by letting $\delta_1 = \delta_2 = 0$ and study the effect of full FLR corrections on TAE and KTAE spectra. We found that both TAE and upper KTAE eigenmodes exist and are undamped, while the lower KTAE is non-existent. Even with finite trapped electron collision the lower KTAE was not found. The upper KTAE mode width in the ballooning θ space is on the order of $1/(sb_{\theta i}^{1/4})$ and is usually much more extended than the TAE mode.

We note that if the leading small FLR correction is kept in the eigenmode equations, Eqs. (28) and (29), discrete eigenmode exist with frequencies below the lower continuum gap boundary. However, these discrete modes are incorrect solutions because their mode structure extends to a large θ domain where $b_{\theta i}(1 + s^2\theta^2) \gg 1$ and the small FLR expansion of the Bessel function breaks down.

The existence of the upper KTAE modes and the non-existence of lower KTAE modes can be understood physically by considering the spatial propagation of kinetic shear Alfvén waves (KAW) [20] of the poloidal harmonics m and $m + 1$ due to FLR effects. For monotonically increasing functions of $q(r)$ and $V_A(r)$, $k_{\parallel}^2 V_A^2$ for the m harmonic increases radially outward for $q(r) > m/n$ and the corresponding KAWs propagate from the field line resonance location r_0 , defined by $\omega^2 = k_{\parallel}^2(r_0)V_A^2(r_0)$, to the smaller $q(r)$ region, but decay exponentially fast in the region $r > r_0$ due to tunneling effects. On the other hand, $k_{\parallel}^2 V_A^2$ for the $(m + 1)$ harmonic increases radially inward in the $q(r) < (m + 1)/n$ region and the corresponding KAWs propagate toward the larger $q(r)$ direction. Therefore, in the $m/n < q(r) < (m + 1)/n$ region the m and $m + 1$ KAWs propagate in opposite directions. For wave frequencies above the continuum gap, the m and $(m + 1)$ KAWs propagate toward each other and can form bound eigenstate of upper KTAE. But, for wave frequencies below the continuum gap, the m and $(m + 1)$ KAWs propagate away from each other and they may interact due to the tunneling effect. In the evanescent region KAWs decay exponentially fast and do not interact effectively to form eigenmodes. Note that in the resistive MHD model [1] the lower and upper PSAWs exist due to the propagation of the m and $(m + 1)$ harmonics as a result of finite resistivity because each harmonic propagates in both directions away from the field line resonance location.

3.2. Collisional-Radiative Damping

Because TAE and KTAE exist in the dissipationless limit, dissipative effects due to electron collision and fast ion drive can be treated perturbatively in the limit of small dissipation. It has been shown that thermal ion FLR effects enhance the collisional damping of the TAE and KTAE modes [4, 5] and we shall call it the collisional-radiative damping. Figure 1 shows the collisional-radiative damping rate of the TAE and $N = 0$ upper

KTAE modes as a function of the trapped electron collisional parameter δ_1 for the fixed parameters $\hat{\epsilon} = 0.2$, $b_{\theta i} = 10^{-4}$, $s = 0.5$, $q = 2$, $\beta_i = 0.01$, $T_e/T_i = 1$, $\epsilon_0 = 0.1$, and $\alpha_{ph} = \alpha_{pc} = \delta_2 = 0$. The thermal ion diamagnetic drift frequency is turned off. For the range of δ_1 presented in Fig. 1 the real frequency of the TAE mode is about $\omega_r/\omega_A = 0.493$ and the real frequency of $N = 0$ upper KTAE mode is about $\omega_r/\omega_A = 0.6$. For $\delta_1 < 10^{-2}$ the damping rates of both TAE and KTAE are linearly proportional to δ_1 and the KTAE damping rate is smaller than the TAE damping rate, where δ_1 is proportional to $\sqrt{\nu_e/\omega}$. But, for $\delta_1 > 10^{-2}$ the TAE damping rate saturates and becomes smaller than the KTAE damping rate. Note that δ_2 provides the collisional-radiative damping through electron pressure response and can be treated perturbatively and is ignored here.

Because the existence of KTAE is due to finite FLR effects, KTAE modes have larger parallel electric field and suffer stronger collisional-radiative damping than TAE modes in the small FLR limit. Figure 2 shows the thermal ion FLR effect on eigenmode frequencies of the TAE and $N = 0$ upper KTAE and TAE modes for $\delta_1 = 0.2$. The thermal ion diamagnetic drift frequency is turned off. The other fixed parameters are the same as in Fig. 1. The real frequency of the TAE mode does not change much with $b_{\theta i}$, while for the $N = 0$ upper KTAE mode ω_r increases with $b_{\theta i}$. The damping rates of the $N = 0$ upper KTAE mode is linearly proportional to $b_{\theta i}$ and is larger than the TAE mode damping rate. However, for $b_{\theta i} > 10^{-4}$ the FLR effect is increasingly important in comparison with the effect of toroidicity and the TAE damping rate is enhanced by the FLR effect. For $b_{\theta i} > 10^{-3}$ the damping rates of the TAE and $N = 0$ upper KTAE modes become comparable.

3.3. Fast Particle Drive and Resonant TAE Modes

Including the fast particle drive the TAE and KTAE modes can be unstable. Figure 3 shows the eigenfrequencies of the TAE and KTAE modes as functions of fast particle drive parameter α_{ph} . The fixed parameters are $T_h/T_i = 200$, $\epsilon_h = 0.1$, $\hat{\epsilon} = 0.2$, $b_{\theta i} = 10^{-4}$, $s = 0.5$, $q = 2$, $T_e/T_i = 0.5$, $\beta_i = 0.02$, $\epsilon_n = 0.2$, $\delta_1 = 0.1$, $\delta_2 = 0.2$, and $\alpha_{pc} = \epsilon_0 = 0$. The growth rates of the TAE and KTAE modes increase, but the real frequency decrease, linearly with α_{ph} . Thus, the effects of fast particles on the stability of the TAE and KTAE modes can be treated perturbatively. From Eq. (29) the growth

rates are proportional to the perturbed pressure which is proportional to $\alpha_{ph}(\omega/\omega_{dh})$. It is clear that the TAE is much more susceptible to the fast particle drive and is much more unstable than the KTAE. The energy exchange between KTAE and fast particles is small mainly due to the poloidally extended wave structure of the KTAE modes due to FLR effects.

Because $\omega_{dh}/\omega_A = qk_\theta \rho_i \beta_i^{1/2} (T_h/T_i)$, the $\omega = \omega_{dh} \mathcal{E}/\mathcal{E}_{h0}$ resonance condition can not be met for small ω_{dh} , where $\mathcal{E} \leq \mathcal{E}_{h0}$. If the TAE and KTAE modes are not in resonance with fast particles, they will be stabilized. The TAE real frequencies and growth rates as a function of the fast particle temperature T_h/T_i are presented in Fig. 4 for $\alpha_{ph} = 0.1$. The other fixed parameters are the same as in Fig. 3. As T_h/T_i decreases, the TAE frequency decreases in order to be in resonance with fast particles, and the growth rate decreases faster reflecting a smaller number of resonance fast particles which is proportional to $(\omega_{dh}/\omega)^{3/2}$. For larger T_h/T_i the number of resonance fast particles increases, but the resonant energy decreases so that the effective perturbed pressures are smaller and the growth rate decreases. We also note from Fig. 4 that for $T_h/T_i < 130$ the TAE frequency moves down into the lower continuum. Because the mode frequency tends to follow the resonant magnetic drift frequency resembling the beam driven mode in the beam-plasma interaction case, we shall call it the resonant TAE mode (RTAE). With larger fast particle drive and smaller ω_{dh} the RTAE frequency can be much below the continuum gap frequency. We note that the resonant RTAE (beam-like modes) can exist with eigenfrequency proportional to the characteristic resonance frequency of fast particles, i.e., magnetic drift or transit or bounce frequencies or their combinations. Because of the beam mode like feature the stability of the RTAE mode must be calculated by a non-perturbative analysis.

3.4. Coupling of TAE, RTAE and Kinetic Ballooning Modes

From Eq. (29) we see that the α_{pc} term, which contains the effect of finite bulk plasma pressure gradient and magnetic field curvature, can significantly reduce the TAE frequency [21] and provides coupling with the kinetic ballooning modes [19, 22, 23]. Fig. 5 shows the effect of α_{pc} on the TAE and KTAE modes. The fixed parameters are $b_{\theta i}$ for $\alpha_{ph} = 0.1$, $T_h/T_i = 200$, $\epsilon_h = 0.1$, $\hat{\epsilon} = 0.2$, $\beta_i = 0.02$, $s = 0.5$, $q = 2$, $T_e/T_i = 0.5$, $\epsilon_n = 0.2$, $\delta_1 = 0.1$,

$\delta_2 = 0.2$. The effect of α_{pc} on the KTAE mode is very small. However, the TAE mode frequency decreases roughly linearly with increasing α_{pc} to well below the lower continuum gap boundary. For $\alpha_{pc} > 0.1$ the TAE frequency moves down into the lower continuum and its growth rate reaches the minimum. As α_{pc} further increases, the mode frequency continues to decrease, but its growth rate starts to increase. We identify the mode as the RTAE mode. For larger α_{pc} the RTAE mode eventually connects to a almost purely growing kinetic ballooning mode. The ideal MHD ballooning instability threshold is about $\alpha_{pc} \simeq 0.4$ for $s = 0.5$. The frequency and the growth rate of the RTAE mode is consistent with observed BAE modes in DIII-D [7], where the fast particle drive is strong and plasma beta is high so that α_{pc} is near the ideal MHD ballooning threshold.

To excite the RTAE mode it requires a larger fast particle drive than the TAE mode. Figure 6 shows the real frequencies and growth rates of the TAE mode for $\alpha_{pc} = 0$ and of the RTAE mode for $\alpha_{pc} = 0.2$ as functions of the fast particle drive parameter α_{ph} . The other fixed parameters are $b_{\theta i} = 10^{-2}$, $T_h/T_i = 150$, $\epsilon_h = 0.1$, $\hat{\epsilon} = 0.2$, $\beta_i = 0.02$, $s = 0.5$, $q = 2$, $T_e/T_i = 0.5$, $\epsilon_n = 0.2$, $\epsilon_0 = 0$, $\delta_1 = 0.1$, $\delta_2 = 0.2$. Note that the RTAE mode exists only at large drive with $\alpha_{ph} > 0.05$. The growth rate of the RTAE is not linear with α_{ph} and requires a non-perturbative analysis.

Figure 7 shows the real frequencies and growth rates of the RTAE mode versus $b_{\theta i}$ for $\alpha_{ph} = 0.1$, $\alpha_{pc} = 0.2$, $T_h/T_i = 150$, $\epsilon_h = 0.1$, $\hat{\epsilon} = 0.2$, $\beta_i = 0.02$, $s = 0.5$, $q = 2$, $T_e/T_i = 0.5$, $\omega_{*i} = \delta_1 = \delta_2 = 0$. The RTAE real frequency roughly keeps track with ω_{dh} , which is proportional to $k_{\theta}\rho_i$. The maximum growth rate occurs at $(\omega_r/\omega_A) \simeq 0.22$, which is much below the lower continuum gap boundary frequency.

4. SUMMARY AND CONCLUSION

A numerical non-perturbative eigenmode analysis has been performed to study the existence of the TAE and KTAE modes as well as the stability properties of the TAE, KTAE, RTAE and kinetic ballooning modes. In the dissipationless limit the upper KTAE mode exists, while lower KTAE branch is shown to be non-existent. Because the TAE and upper KTAE modes exist in the dissipationless limit, the effect of dissipation on their stability can be studied by a perturbative method in the small dissipation limit. The

TAE mode is found to be strongly destabilized by fast ions because the fast particle drive is usually much larger than the collisional-radiative damping rates. The upper KTAE mode is usually stable and can at most be marginally unstable even with very strong fast ion drive. The upper KTAE mode suffers a stronger collisional-radiative damping than the TAE mode because the KTAE mode has a larger k_{\perp} than the TAE mode and, therefore, a larger parallel electric field.

A beam-like resonant type TAE (RTAE) mode also exists with frequency proportional to the fast particle magnetic drift frequency or bounce/transit frequency or their combination. The RTAE mode can be excited at high total plasma pressure and large fast particle drive. As the plasma β increases, the TAE frequency decreases and changes into a RTAE mode which has a real frequency much below the lower Alfvén continuum gap boundary. As the plasma β increases further near the ideal MHD β threshold, the RTAE mode connects to a kinetic ballooning mode. A non-perturbative stability analysis is essential for the RTAE mode and its coupling to the kinetic ballooning mode. The growth rate and real frequency of the RTAE mode is consistent with the BAE mode experimentally observed in DIII-D.

ACKNOWLEDGMENTS

This work was supported by the United States Department of Energy under Contract No. DE-AC02-CHO-3073.

References

- [1] CHENG, C. Z., CHEN, L., and CHANCE, M. S., Ann. Phys. NY **161** (1985) 21.
- [2] CHENG, C. Z. and CHANCE, M. S., Phys. Fluids **29** (1986) 3695.
- [3] METT, R. and MAHAJAN, S., Phys. Fluids B **4** (1992) 2885.
- [4] BERK, H. L., METT, R. R., and LINDBERG, D. M., Phys. Fluids B **5** (1993) 3969.
- [5] CANDY, J. and ROSENBLUTH, M. N., Phys. Plasmas **1** (1994) 356.
- [6] HEIDBRINK, W. W., STRAIT, E. J., CHU, M. S., and TURNBULL, A. D., Phys. Rev. Lett. **71** (1993) 855.
- [7] HEIDBRINK, W. W. and SADLER, G. J., Nucl. Fusion **34** (1994) 535.
- [8] FU, G. Y. and CHENG, C. Z., Phys. Fluids B **4** (1992) 3722.
- [9] HEIDBRINK, W. W., STRAIT, E. J., DOYLE, E., SAGER, G., and SNIDER, R., Nucl. Fusion **31** (1991) 1635.
- [10] WONG, K. L., FONCK, R. J., PAUL, S. F., et al., Phys. Rev. Lett. **66** (1991) 1874.
- [11] CHENG, C. Z., Phys. Rev. **211** (1992) 1.
- [12] ANTONSEN, T. M. and LANE, B., Phys. Fluids **23** (1980) 1205.
- [13] CATTO, P. J., TANG, W. M., and BALDWIN, D. E., Plasma Phys. **23** (1981) 639.
- [14] GORELENKOV, N. N. and SHARAPOV, S. E., Physica Scripta **45** (1991) 163.
- [15] ROSENBLUTH, M. N., ROSS, D. W., and KOSTOMAROV, D. P., Nucl. Fusion **12** (1972) 3.
- [16] MIKHAILOVSKII, A. B., in *Reviews of Plasma Physics*, edited by M. A. Leontovich, volume 9, Consultants Bureau, New York, 1986.

- [17] CONNOR, J. W., HASTIE, R. J., and TAYLOR, J. B., Proc. Roy. Soc. Lon. A **365** (1979) 1.
- [18] DEWAR, R. L., MANICKAM, J., GRIMM, R. C., and CHANCE, M. S., Nucl. Fusion **21** (1981) 493.
- [19] CHENG, C. Z., Nucl. Fusion **773** (1982) 22.
- [20] HASEGAWA, A. and CHEN, L., Phys. Rev. Lett. **36** (1976) 1362.
- [21] FU, G. Y. and CHENG, C. Z., Phys. Fluids B **2** (1990) 985.
- [22] CHENG, C. Z., Phys. Fluids **25** (1982) 1020.
- [23] TSAI, S. and CHEN, L., Phys. Fluids B **5** (1993) 3284.

Collisional-Radiative Damping

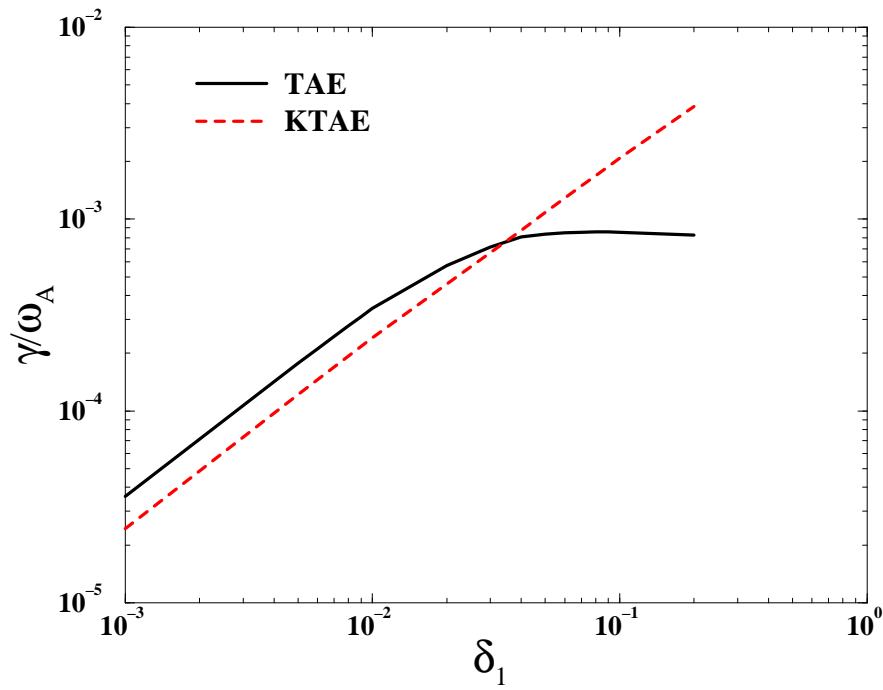


Figure 1: The collisional-radiative damping rates of the TAE and $N = 0$ upper KTAE modes versus the trapped electron collisional parameter δ_1 .

Collisional-Radiative Damping

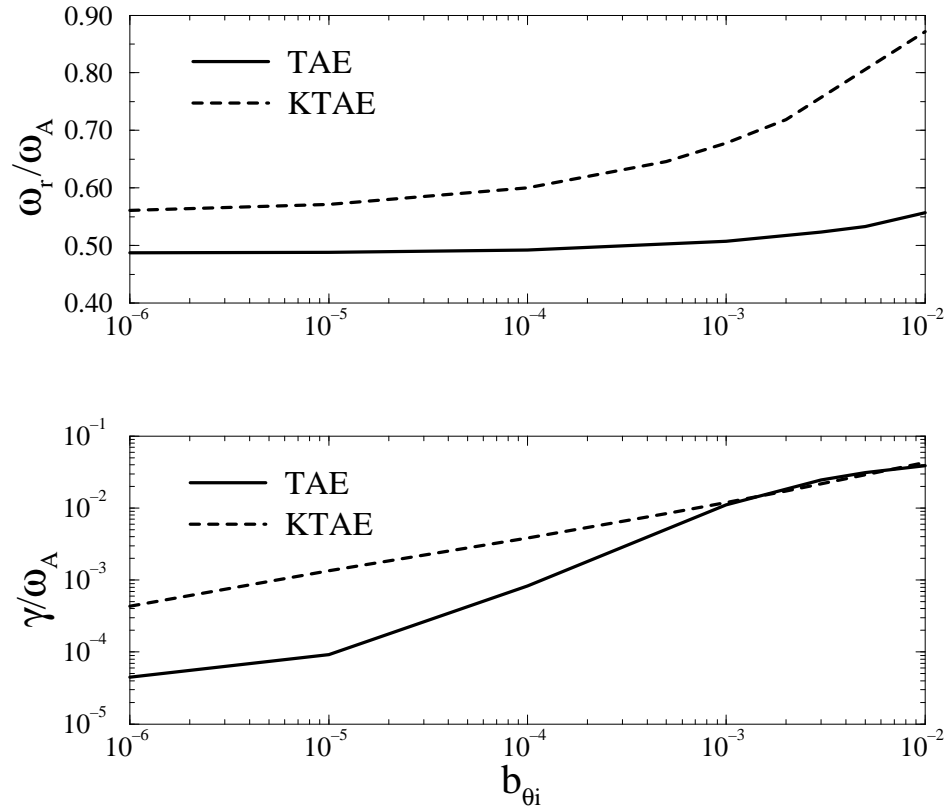


Figure 2: The dependence of the real frequencies and collisional-radiative damping rates of the TAE (solid curves) and KTAE (dashed curves) modes on the thermal ion FLR parameter $b_{\theta i}$.

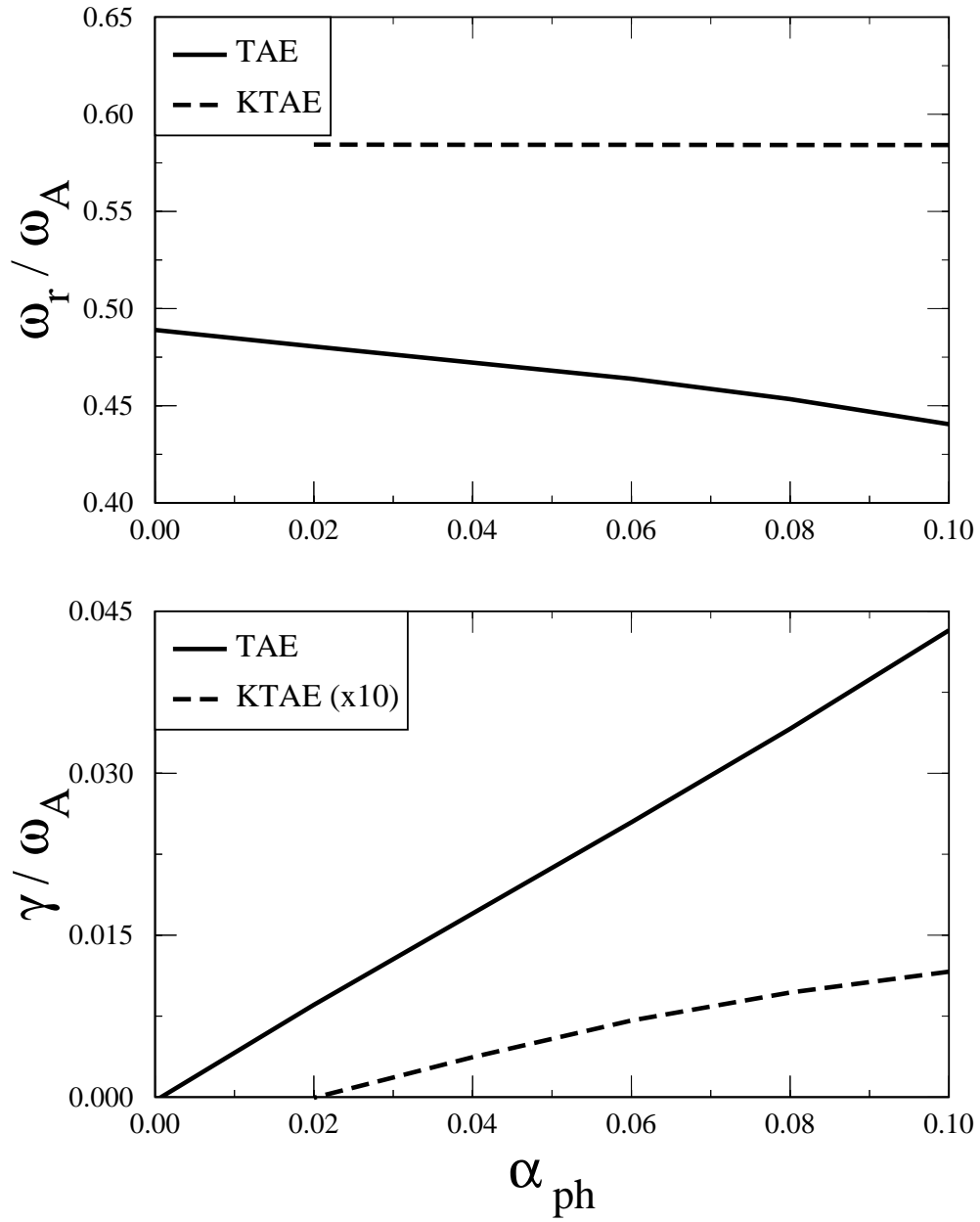


Figure 3: The real frequencies and growth rates of the TAE and KTAE modes versus the fast particle drive parameter α_{ph} .

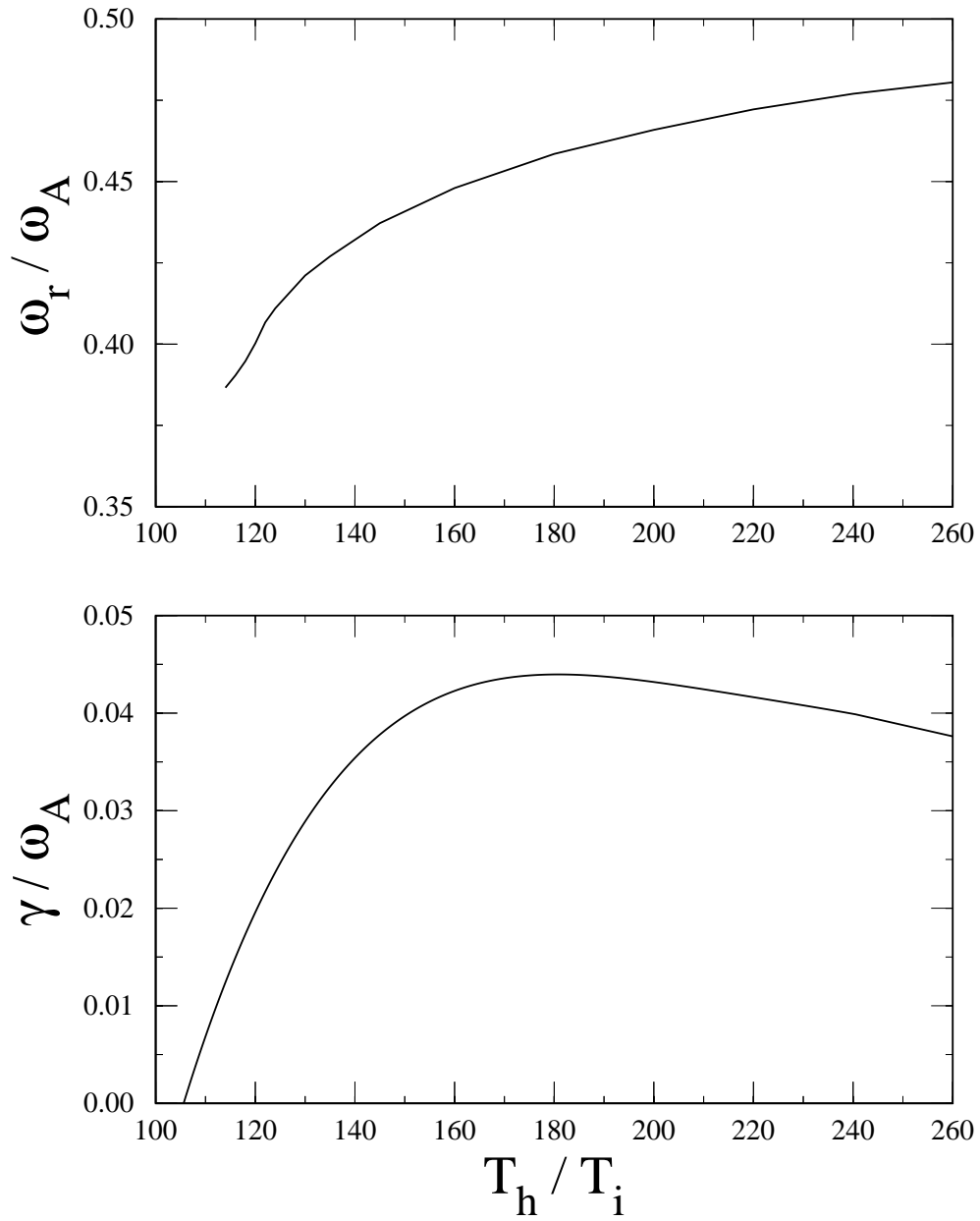


Figure 4: The real frequency and growth rate of the TAE mode versus the fast particle temperature T_h/T_i .

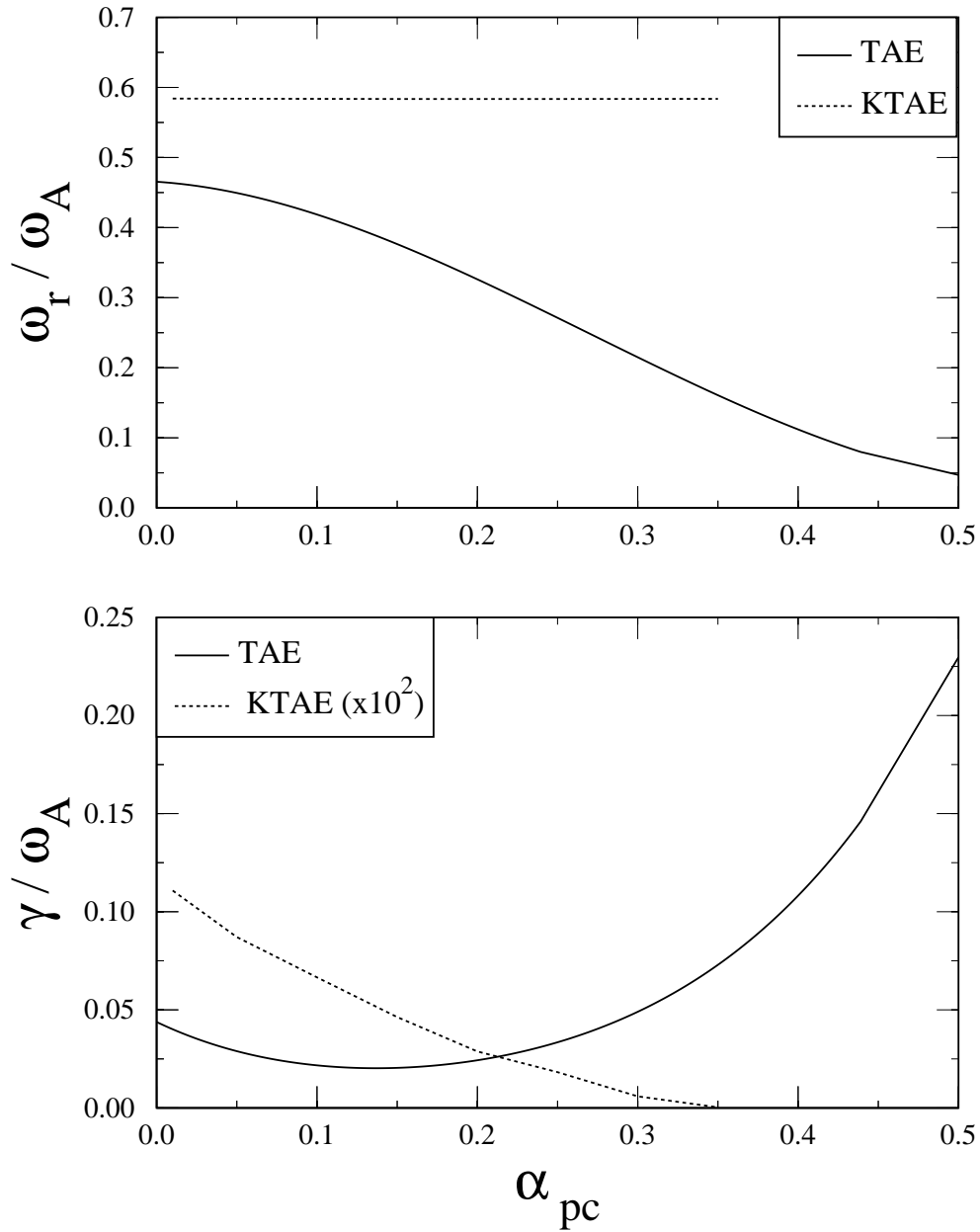


Figure 5: The real frequencies and growth rates of the TAE and KTAE modes versus the bulk plasma pressure parameter α_{pc} . As α_{pc} increases, the TAE mode moves into a RTAE mode and eventually connects to a kinetic ballooning mode.

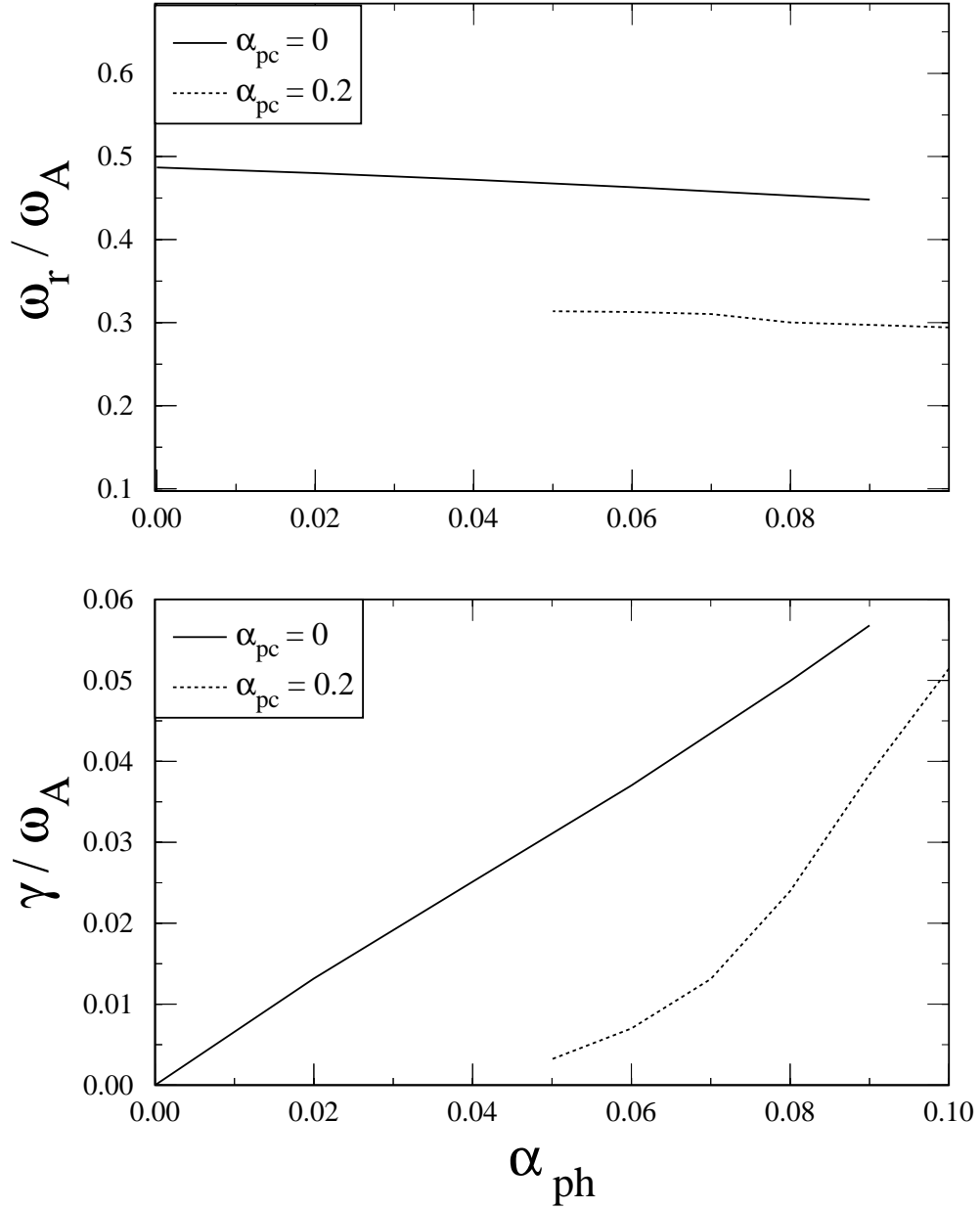


Figure 6: The real frequency and growth rates of the TAE mode for $\alpha_{pc} = 0$ and of the RTAE mode for $\alpha_{pc} = 0.2$ versus the fast particle drive parameter α_{ph} .

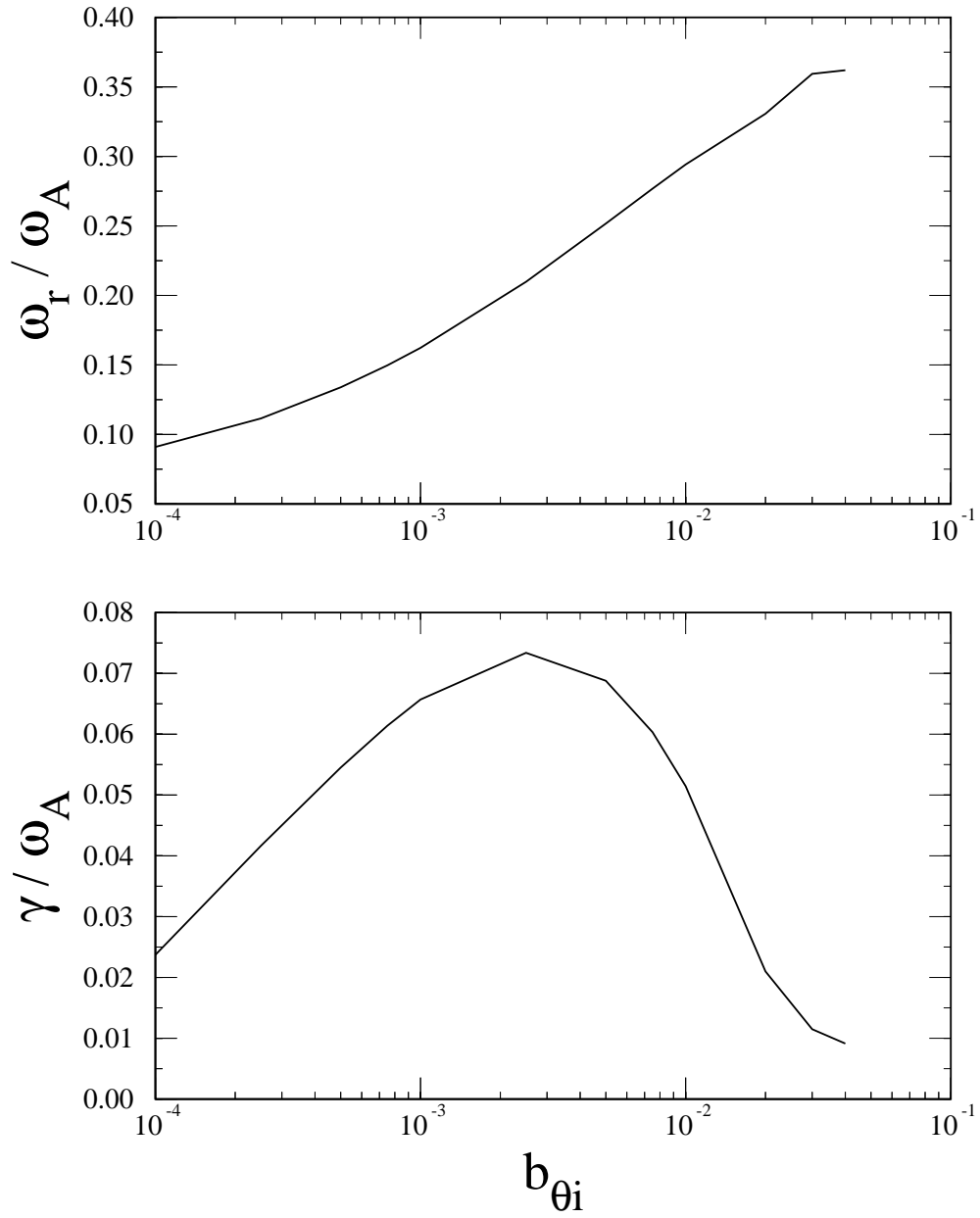


Figure 7: The effect of ion FLR parameter $b_{\theta i}$ on the RTAE mode real frequency and growth rate. The RTAE real frequency roughly follows ω_{dh} , which is proportional to $k_{\theta} \rho_i$.